Combining a Reduced Field of Excitation With SENSE-Based Parallel Imaging for Maximum Imaging Efficiency

Ronald Mooiweer,* Alessandro Sbrizzi, Alexander J.E. Raaijmakers, Cornelis A.T. van den Berg, Peter R. Luijten, and Hans Hoogduin

Purpose: To show that a combination of parallel imaging using sensitivity encoding (SENSE) and inner volume imaging (IVI) combines the known benefits of both techniques. SENSE with a reduced field of excitation (rFOX) is termed rSENSE.

Theory and Methods: The noise level in SENSE reconstructions is reduced by removing voxels from the unfolding process that are rendered silent by using rFOX. The silent voxels need to be identified beforehand, this is done by using rFOX in the coil sensitivity maps. In vivo experiments were performed at 7 Tesla using a 32-channel receive coil.

Results: Good image quality could be obtained in vivo with rSENSE at acceleration factors that are higher than could be obtained using SENSE or IVI alone. With rSENSE we were also able to accelerate scans using an rFOX that was purposely designed to be imperfect or incompatible at all with IVI.

Conclusion: rSENSE has been demonstrated in vivo with two-dimensionally selective radiofrequency pulses. Besides allowing additional scan acceleration, it offers a greater robustness and flexibility than IVI. The proposed method can be used with other field strengths, anatomies and other rFOX techniques.

Key words: parallel imaging; reduced field of excitation; inner volume imaging; voxel exclusion

INTRODUCTION

Ever since the introduction of MRI, there has been a quest for methods that can shorten the image acquisition time. Both inner volume imaging (IVI) (2) and parallel imaging (PI) (3,4) are examples of nonsequence-specific techniques that can be used to achieve this. In addition, these techniques improve image quality in sequences where T_2/T_2^* decay causes blurring and distortions, by shortening the readout times (5–7). Furthermore, using IVI, movement artifacts can be avoided by not exciting (moving) areas outside the region of interest (ROI) (8,9). These techniques are especially interesting for ultrahigh field imaging ($\geq$7T) where an increased signal-to-noise ratio (SNR) allows for high resolution imaging, accompanied with prolonged scan-times and an amplification of the aforementioned image artifacts.

In recent years, the realization arose that IVI, and in particular the signal-localization techniques that are used to facilitate this, could be used to improve PI. This is shown by several papers where an improved PI performance is described when the signal generating area was reduced in specific applications (10–15). Most notable is the work on zoomed GRAPPA (ZOOPPA) (10), where the signal in a part of the FOV is suppressed such that high GRAPPA acceleration factors can be used to achieve high resolution fMRI (12) and DWI (11) of the remaining areas. The authors of the former publication also noted that GRAPPA can be used to (retrospectively) reconstruct the full FOV from IVI images in cases where signal suppression was imperfect, which would otherwise lead to aliasing of this unwanted signal into the region of interest. An interesting take on the subject matter is provided by Taviani et al. who introduced the concept of virtual coil profiles for the combined use of a multiband excitation pattern with PI (15).

To effectively discuss the decoupling of IVI from the enabling techniques that limit the signal generating area, we introduce the term reduced field of excitation (rFOX). In this terminology, IVI is the combined use of rFOX and a reduced field of view (rFOV) (Fig. 1e). Here, rFOV is any encoded FOV that is smaller than the full FOV, usually matching the size and shape of the rFOX. The full FOV is the fully encoded FOV such that no aliasing occurs when a regular (1D selective) excitation is used. The method by which the rFOX is created is not relevant for the definition of the concept.

Up to now, a detailed analysis of the interactions between rFOX and PI is missing, obscuring the potential applicability of the combination of these techniques. In the current work, we combine rFOX with SENSE (16,17). Because SENSE operates in the image domain instead of the k-space domain (GRAPPA) (18), it simplifies the conceptual and theoretical explanation of rFOX with PI.

Center for Image Sciences, University Medical Center Utrecht, Utrecht, The Netherlands.

*Correspondence to: Ronald Mooiweer, MSc., Heidelberglaan 100, 3508 GA Utrecht, The Netherlands. E-mail: r.mooiweer@umcutrecht.nl; Twitter: @mooiweerr

Received 31 March 2016; revised 23 June 2016; accepted 24 June 2016

DOI 10.1002/mrm.26346

Published online 16 September 2016 in Wiley Online Library (wileyonlinelibrary.com).

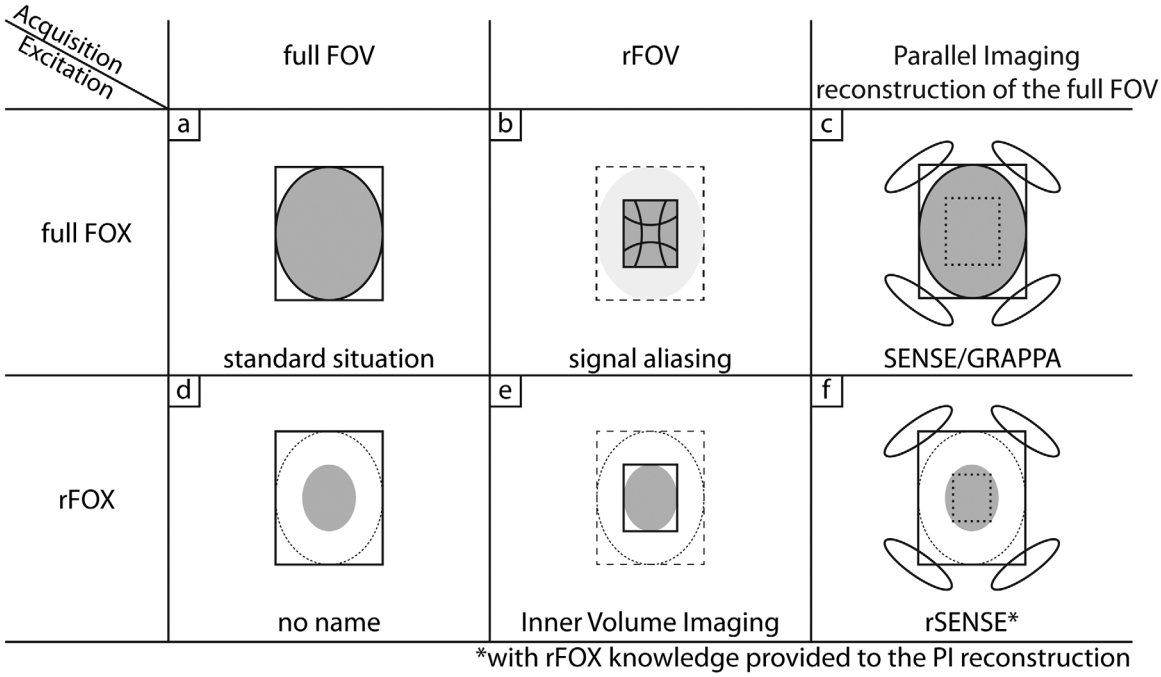

FIG. 1. Summary of different combinations of full and reduced FOV, FOX, and PI.

We argue that, instead of combining rFOX with rFOV into IVI, or even applying PI on the rFOV acquired by IVI, PI alone is the preferred method to be combined with rFOX. When used correctly, PI gives an increased robustness towards imperfect suppression of signal outside the targeted ROI and in general a greater flexibility by allowing accelerated imaging of rFOX shapes that are incompatible with rFOV imaging. In particular, the combination of rFOX and SENSE is dubbed rSENSE, and is explained in detail in this manuscript. Several examples of rSENSE accelerated scans are given using subject-specific two-dimensionally selective radiofrequency (2D RF) pulses (19,20) to create the rFOX. This study has been presented in part at the annual meeting of the ISMRM in Toronto, Canada, in 2015 (1).

THEORY

The different ways in which a reduced field of excitation can be combined with a reduction of the acquired FOV or parallel imaging are schematically reported in Figure 1. To understand the effect rFOX has on SENSE, we will briefly recapitulate the theory of SENSE (4). In particular, the way in which noise is propagated during SENSE reconstruction. The basic principle of SENSE is the unfolding of aliased voxel-values using coil sensitivity information. Compared with a fully (Nyquist) encoded FOV (Fig. 1a), the density of the regularly sampled k-space lines is reduced by an acceleration factor R, shortening the acquisition by the same factor. Effectively, the encoded FOV is reduced by R as well, leading to R voxels aliasing (collapsing) onto each other, at every location in the reduced FOV (Fig. 1b).

This accumulated signal is detected by multiple coils simultaneously and needs to be unfolded to create an image of the full FOV (Fig. 1c). The detected, aliased, signal per receive channel is assembled into a vector $\boldsymbol{\sigma}$ whose length is the number of receive coils (N_{coils}). It follows that $\boldsymbol{\sigma} = \mathbf{S}\,\boldsymbol{\rho}$, with $\mathbf{S}$ the $N_{coils} \times R$ coil sensitivity matrix and $\boldsymbol{\rho}$ the true signal originating from the aliasing voxels (vector of length R). The true signal can be retrieved in a least squares sense by means of $\boldsymbol{\rho} = \left(\mathbf{S}^{\mathrm{H}}\mathbf{S}\right)^{-1}\mathbf{S}^{\mathrm{H}}\,\boldsymbol{\sigma}$. The condition number of the matrix $\mathbf{S}$ describes how much the calculated value $\boldsymbol{\rho}$ changes with a small change in $\boldsymbol{\sigma}$. Small changes in $\boldsymbol{\sigma}$ occur naturally and are randomly distributed across the image (noise), so an amplification of noise will occur when the problem is ill-conditioned. The level of noise amplification in each voxel depends on the spatial variation of the receive coil sensitivities and is represented by the geometry factor (g-factor).

When the noise correlation matrix between receive coils $\boldsymbol{\Psi}$ is also taken into account, the g-factor is defined as $g_j(\mathrm{R}) = \sqrt{\left[\left(\boldsymbol{S}^{H}\boldsymbol{\Psi}^{-1}\boldsymbol{S}\right)^{-1}\right]_{j,j}\left(\boldsymbol{S}^{H}\boldsymbol{\Psi}^{-1}\boldsymbol{S}\right)_{j,j}}$ (4), at voxel location j. The g-factor is related to the SNR in a SENSE-accelerated image, compared with a fully sampled acquisition, by means of $SNR_{SENSE}(R) = SNR_{full}/\left(g\sqrt{R}\right)$. The $\sqrt{R}$ term follows from the reduced number of Fourier averaged samples contributing to the total SNR. This loss mechanism equally affects rFOV sequences without parallel imaging, such as IVI (Fig. 1e): $SNR_{IVI}(R) = SNRfull/\sqrt{R}$. For ideal SENSE unfolding, so without amplification of noise, g equals 1. Because in practice $g > 1$, the SNR in a scan using IVI will be higher than when SENSE is used to achieve the same scan acceleration factor. In contrast to IVI, however, SENSE will reconstruct the full FOV and not just the rFOV.

In the here-proposed rSENSE method (Fig. 1f), rFOX is used to reduce the number of aliasing voxels at a given acceleration factor R. The reduced number of aliasing

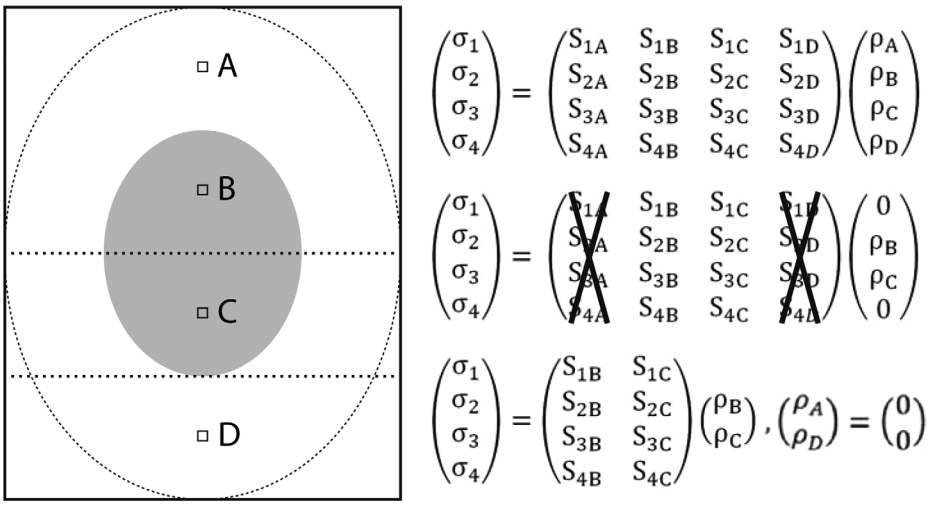

$$\begin{pmatrix}\sigma_1\\ \sigma_2\\ \sigma_3\\ \sigma_4\end{pmatrix} = \begin{pmatrix}S_{1A} & S_{1B} & S_{1C} & S_{1D}\\ S_{2A} & S_{2B} & S_{2C} & S_{2D}\\ S_{3A} & S_{3B} & S_{3C} & S_{3D}\\ S_{4A} & S_{4B} & S_{4C} & S_{4D}\end{pmatrix}\begin{pmatrix}\rho_A\\ \rho_B\\ \rho_C\\ \rho_D\end{pmatrix}$$

$$\begin{pmatrix}\sigma_1\\ \sigma_2\\ \sigma_3\\ \sigma_4\end{pmatrix} = \begin{pmatrix}\cancel{S_{1A}} & S_{1B} & S_{1C} & \cancel{S_{1D}}\\ \cancel{S_{2A}} & S_{2B} & S_{2C} & \cancel{S_{2D}}\\ \cancel{S_{3A}} & S_{3B} & S_{3C} & \cancel{S_{3D}}\\ \cancel{S_{4A}} & S_{4B} & S_{4C} & \cancel{S_{4D}}\end{pmatrix}\begin{pmatrix}0\\ \rho_B\\ \rho_C\\ 0\end{pmatrix}$$

$$\begin{pmatrix}\sigma_1\\ \sigma_2\\ \sigma_3\\ \sigma_4\end{pmatrix} = \begin{pmatrix}S_{1B} & S_{1C}\\ S_{2B} & S_{2C}\\ S_{3B} & S_{3C}\\ S_{4B} & S_{4C}\end{pmatrix}\begin{pmatrix}\rho_B\\ \rho_C\end{pmatrix}, \begin{pmatrix}\rho_A\\ \rho_D\end{pmatrix} = \begin{pmatrix}0\\ 0\end{pmatrix}$$

FIG. 2. Illustration and matrix representation of aliasing voxels (A–D) in a 4× under sampled acquisition with 4 receive coils (1–4). By changing the excitation from the full area (dotted ellipse) to a reduced field of excitation (filled gray ellipse) the signal contributions of voxels A and D vanish. In the corresponding matrix, ρ_A and ρ_D are set to 0, allowing the removal of columns $S_{[1-4],A}$ and $S_{[1-4],D}$ from the equation.

voxels (R_r) can be described using $R_r = R \times \frac{PE_{rFOX}}{PE_{fullFOX}}$, where PE_{rFOX} and $PE_{fullFOX}$ are the number of excited voxels in the phase encoded directions using rFOX and full FOX respectively. In the unfolding procedure, the voxels that do not contribute any signal can be assigned a zero value in **ρ** and the columns of **S** corresponding to the coil sensitivities of these suppressed voxels can be removed from the matrix.

Figure 2 illustrates this situation, where an rFOX is used to reduce the number of aliased voxels from four (A–D) to two (B and C only). Because the number of unknowns is reduced from $R = 4$ to $R_r = 2$, and the number of equations remains the same ($N_{coils} = 4$), the system of equations is typically better conditioned. This is expressed in a lower condition number and g-factors, and results thus into a higher local SNR compared with excitation of the full FOV. An ideal unfolding situation can even be obtained when the size of the rFOX is the same as the rFOV obtained during SENSE acceleration. In this situation of matched excitation reduction and acceleration factor, there is no aliasing of signal, g equals 1, and the SNR of IVI and rSENSE should be equal. Acceleration beyond the ideal unfolding situation, while keeping the rFOX fixed, is possible using rSENSE (with an increased g-factor), though with IVI this would lead to signal aliasing without the ability to unfold it.

METHODS

Identification of Voxels for Exclusion

Because rSENSE works by excluding "silent" voxels from the inversion problem, we need to identify these voxels beforehand. In fact, voxels that lie outside the imaged object are already excluded to improve SNR in regular SENSE (4). In the general implementation of SENSE, these voxels outside the body are easily identified on the separately acquired, 1D-selective, coil sensitivity maps. In our implementation of rSENSE, low flip angle 2D RF pulses are used to create the rFOX. The coil sensitivity mapping scan is in fact a low flip angle gradient echo sequence. So we can simply use the same 2D RF pulses in the mapping sequence to create the rFOX and identify the signal-suppressed voxels inside the object in the same way as the voxels outside the body.

Experimental Validation of rSENSE

A model situation was chosen to experimentally verify the rSENSE method, based on a 3D brain scan in sagittal orientation. An rFOX of 1/3rd the size of the head in both the phase encoding directions (AP and RL) was chosen (dubbed rFOX shape 1). This geometry allows the comparison of scan acceleration in two dimensions by means of rSENSE (Fig. 1f), regular SENSE (Fig. 1c), and IVI (Fig. 1e). Additionally, rFOX was used in combination with SENSE unfolding using sensitivity maps of the full FOX, to show the incompatibility of this combination.

Different 2D acceleration factors were used in the acquisitions: $2 \times 2 = 4$, $3 \times 3 = 9$, $4 \times 4 = 16$, and $5 \times 5 = 25$. The IVI scan was acquired at an rFOV matching the rFOX, so at a 2D reduction factor of $3 \times 3 = 9$, compared with the full FOV. G-factor maps were generated to predict the performance of the SENSE and rSENSE accelerated scans.

To show the robustness of rSENSE toward an imperfect rFOX, compared with IVI, a separate experiment was performed. Here an extra excitation 'hotspot' was added to the design of the 2D RF pulses, outside rFOX shape 1, to simulate imperfect signal suppression (rFOX shape 2).

To show how rSENSE is flexible in accelerating acquisitions of different rFOX shapes that are incompatible with IVI, another additional experiment was performed. Here, the outer cortex was targeted as the ROI in RF pulse design, resulting in a ring-like rFOX with suppression of signal in the center of the brain (rFOX shape 3).

General Scan Parameters

All experiments were performed on a 7 Tesla (T) MRI system (Philips Healthcare, Cleveland, OH) using a 2-channel transmit coil and a 32-channel receive coil (both from Nova Medical, Wilmington, MA). Healthy volunteers were scanned, after having provided informed

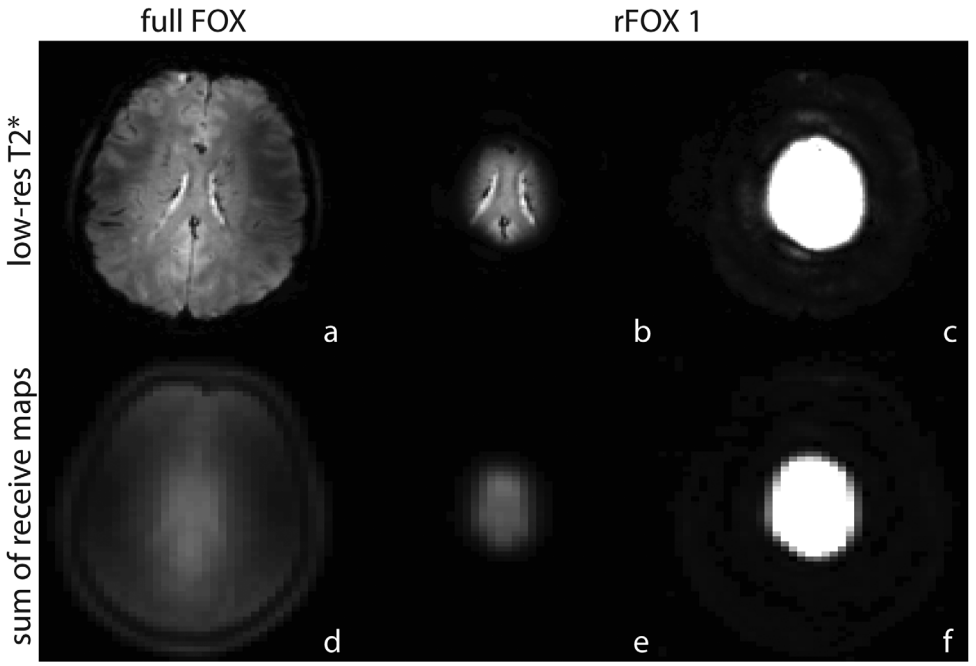

FIG. 3. Full FOX (a,d) and rFOX 1 (b,c,e,f) applied to T2*-weighted images (a–c) and the receive coil sensitivity maps (summed signal, d–f). Panels c and f show the same data as b and e, but with a different intensity window to reveal low intensity signals.

consent. A modified version of the 3D whole-brain protocol for 7T (21) was used. This gradient echo based sequence was chosen for its clinically relevant T_2*-weighted contrast and 0.5 mm isotropic resolution, to facilitate the visual detection of changes in image quality. An EPI acceleration factor of 9 was used to keep scan times short, so that multiple scans using different acceleration methods could be acquired from the same subject. Other scan parameters were: sagittal orientation; FOV, 210 × 210 × 180 mm (FH × AP × RL); repetition time (TR), 75 ms; echo time (TE), 25 ms; flip angle (FA), 15°. Care was taken to disable any oversampling in the phase encoding directions (AP and RL).

Details on rFOX Generation and Coil Sensitivity Mapping

The 2D selective RF pulses were designed on-site using the numerical pulse design method described by Sbrizzi et al. (22). B_1^+ and B_0 information of a transverse slice at approximately half the FH length of the brain was used. B_1^+ maps were acquired using the DREAM method (23), with STEAM flip angle 40°. B_0 maps were acquired using a ΔTE of 1.0 ms. The 2D RF pulses for rFOX shapes 1 and 2 were designed on a spiral-in k-space trajectory with a maximum value of 3 cm/rad, and a duration of 4.3 ms. For rFOX shape 3 a maximum k-space value of 5 cm/rad was chosen, leading to a duration of 8.9 ms.

The sensitivity maps of the receive coils were based on coarse-resolution, proton density weighted, gradient echo scans. The maps were acquired in the standard 1D-selective way, and using the rFOX excitation pulses scaled down to FA = 1°. Compared with the 1D selective scan, the TR was extended from 8 to 18 ms to fit the longer excitation pulses (39 ms for rFOX shape 3). To cross-check the efficacy of the 2D RF pulses in the sensitivity mapping sequence, we acquired a low-resolution $(1.5\ \text{mm})^3$, T_2*-weighted, image without SENSE acceleration (SENSE 1 × 1).

The coil sensitivity maps were conventionally acquired at an overly large FOV to facilitate a wide range of user-desired FOVs and oversampling factors. To correctly calculate the g-factor maps for the FOV used in the (r)SENSE accelerated scans, a set of sensitivity maps was also acquired using this FOV and orientation.

Image Reconstruction

Raw data of the T_2*-weighted scans was saved in the k-space domain and reconstructed offline using ReconFrame (GyroTools LLC, Winterthur, Switzerland). The standard pipeline for SENSE unfolding was used, which included regularization (24). Additionally, the "Mask" option of ReconFrame was enabled during reconstruction of the rSENSE accelerated scans to make sure that the silent voxels obtained with rFOX were excluded from the unfolding process. The "Mask" option is designed to mask out noise only regions from the sensitivity maps and was used without any adjustments.

RESULTS

rSENSE Acceleration of a Centered rFOX

The efficacy of rFOX generation using 2D RF pulses is shown in Figure 3, for shape 1. In the SENSE reconstruction process, the summation of the receive coil sensitivity images is used to determine the voxels that are to be excluded from reconstruction. Because of the matching signal generating areas in the T2* weighted scan and the summed coil sensitivity map, we expect adequate identification of the large number of silent voxels in rSENSE reconstruction.

Figure 4 shows the g-factor maps for increasing acceleration factors (AFs), using SENSE and rSENSE with

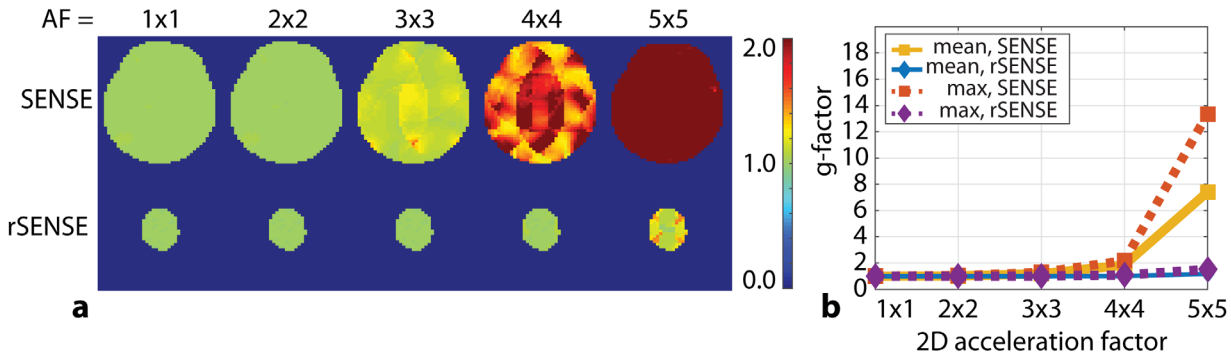

FIG. 4. G-factor maps (a) calculated for acceleration in both phase encoded directions, for SENSE and rSENSE with rFOX shape 1. The mean and maximum values inside the ROI are plotted (b).

rFOX shape 1. At AF = 2 × 2, the g-factor is still close to 1 for both methods. At AF = 3 × 3, a divergence between the g-factors can be seen, and slight difference in SNR can be expected. For AF = 4 × 4 and 5 × 5, g is much higher for SENSE compared with rSENSE. At these acceleration factors, we expect to see substantial SNR differences, resulting in inadequate (using SENSE) and usable (using rSENSE) T_2* weighted images. These AFs cannot be obtained when IVI is used with this rFOX: this would be limited to a FOV reduction of 3 × 3.

In Figure 5, we see how the image quality of rSENSE accelerated images compares with the other acceleration methods of the T_2* weighted acquisitions. The regular SENSE accelerated scan shows signs of image quality

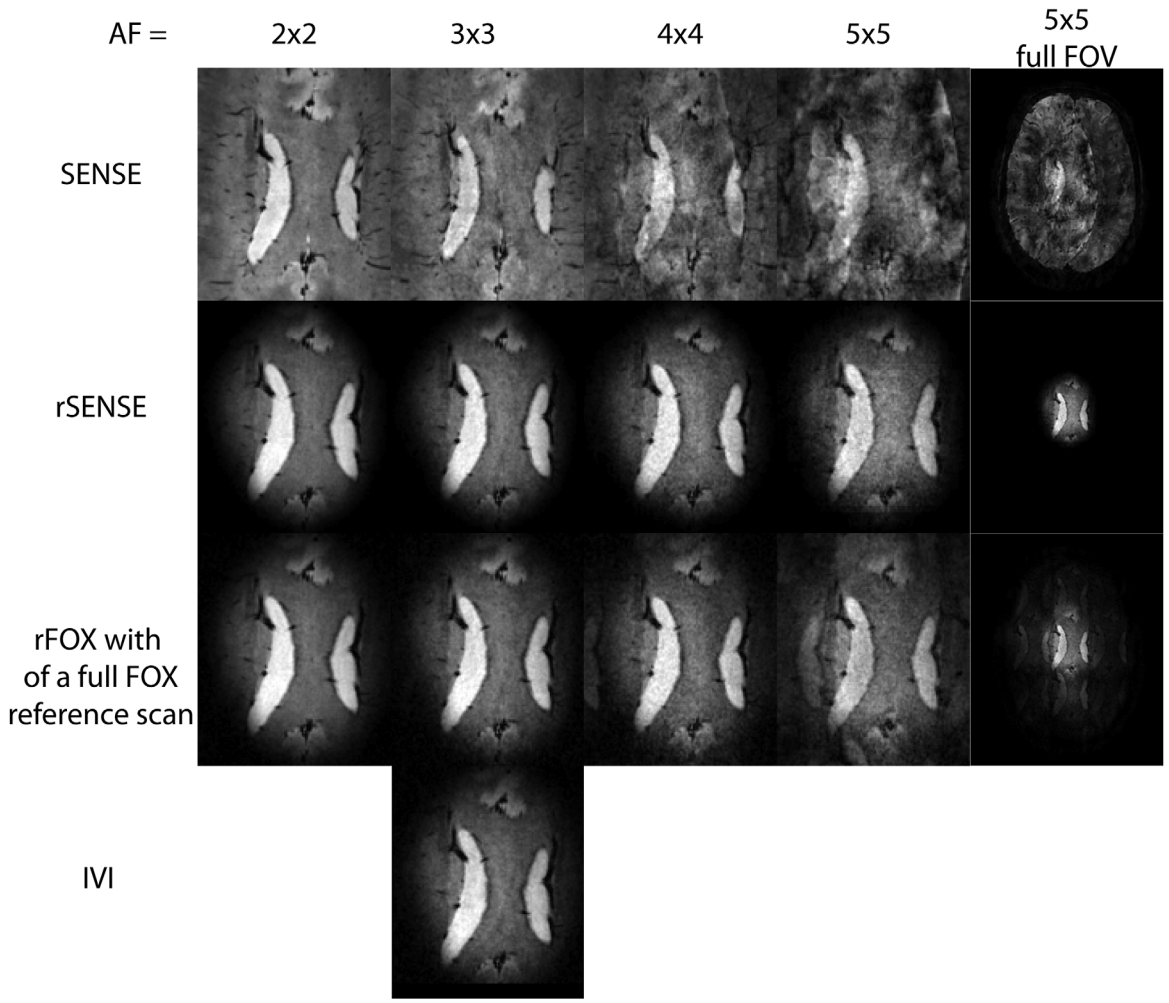

FIG. 5. Transversely reconstructed T_2*-weighted images, showing the corpus callosum in one volunteer. SENSE, rSENSE, and SENSE unfolding of rFOX using a full FOX reference scan are used at increasing acceleration factors. The column on the right shows the full FOV image for anatomical reference, the other columns are zoomed images to show the ROI. IVI using an rFOV of 1/3rd × 1/3rd the size of the full FOV is also shown.

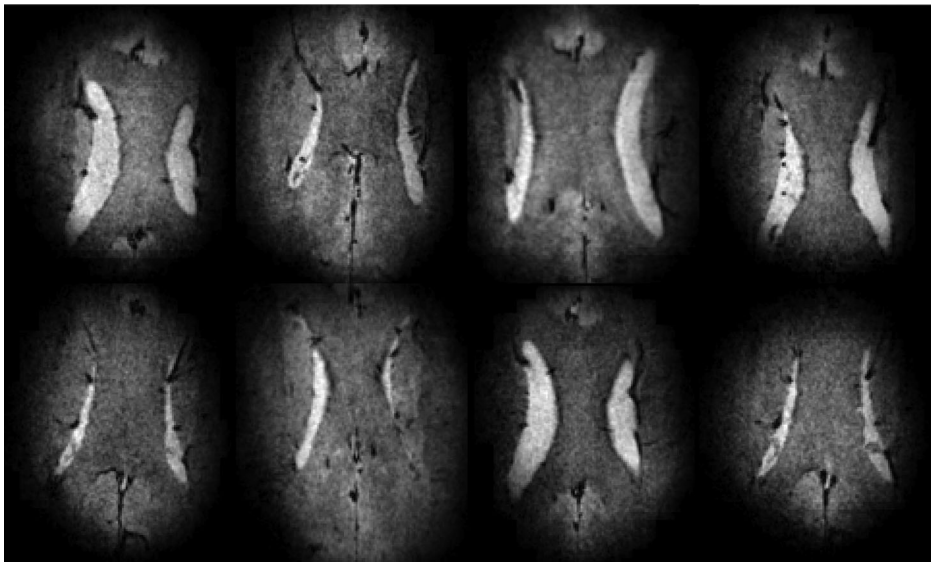

FIG. 6. rSENSE accelerated, T_2*-weighted, images of the corpus callosum in eight volunteers. AF = 5 × 5, rFOX shape 1 = 1/3 × 1/3 of full FOX. The images are transverse reconstructions form the sagitally acquired 3D scans, and zoomed to show the ROI.

degradation already at AF = 3 × 3, and artifacts are dominating the images' appearance at higher acceleration factors. When rFOX is used, the image quality at 3 × 3 times undersampling is comparable for all techniques. This includes the IVI image, confirming that rSENSE and IVI are equivalent when the $g = 1$ situation is realized. Furthermore, no noticeable artifacts are introduced at rSENSE acceleration factors of 4 × 4 and 5 × 5, only an increase in noise can be observed, as is expected from the $1/\sqrt{R}$ relationship with SNR.

When rFOX is used in combination with SENSE unfolding using a full FOX reference scan, we see that signal is incorrectly allocated to locations outside the targeted rFOX, at AF = 4 × 4 and 5 × 5. This can be seen in the zoomed reproductions, and even more in the full FOV images.

Figure 6 shows that rSENSE constantly provides good image quality when the experiment is repeated in multiple volunteers. Some variation in size and shape of the rFOX can be seen, partly corresponding to variations in head size between volunteers and partly due to inconsistencies in the manual planning of the rFOX.

In Figure 7, we see transverse slices reconstructed at a lower position in the brain, showing the red nuclei and substantia nigra. Noteworthy here is that the SENSE accelerated images have severe artifacts whereas in the rSENSE accelerated images the actual brain structures can be seen. The banding artifacts originate from the rapid susceptibility changes near the nasal cavities. Because of intentional aliasing followed by SENSE unfolding, the artifacts are repeated across the full FOV, also into the ROI. When rSENSE is used, the locations that generate the artifacts are mostly outside the rFOX, thus preventing signal generation in this area of rapid susceptibility changes in the first place. Useful images were created with rSENSE acceleration, even though these basal ganglia are in a very challenging location because of pulsating motion associated with the lower brain region.

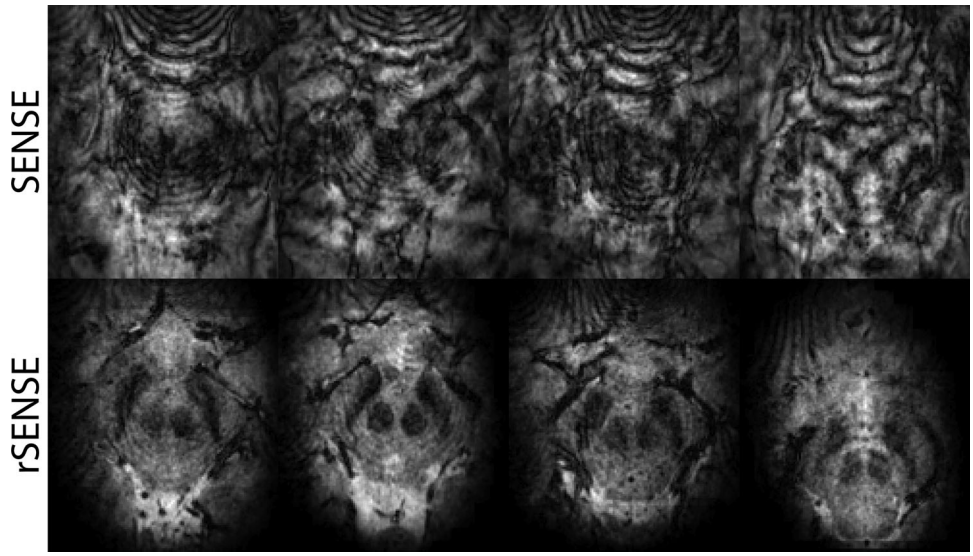

FIG. 7. T_2*-weighted images using SENSE (top row) and rSENSE (bottom row) at 5 × 5 acceleration factor in four different volunteers. Transverse, zoomed in, slices are reproduced, showing the red nuclei and substantia nigra.

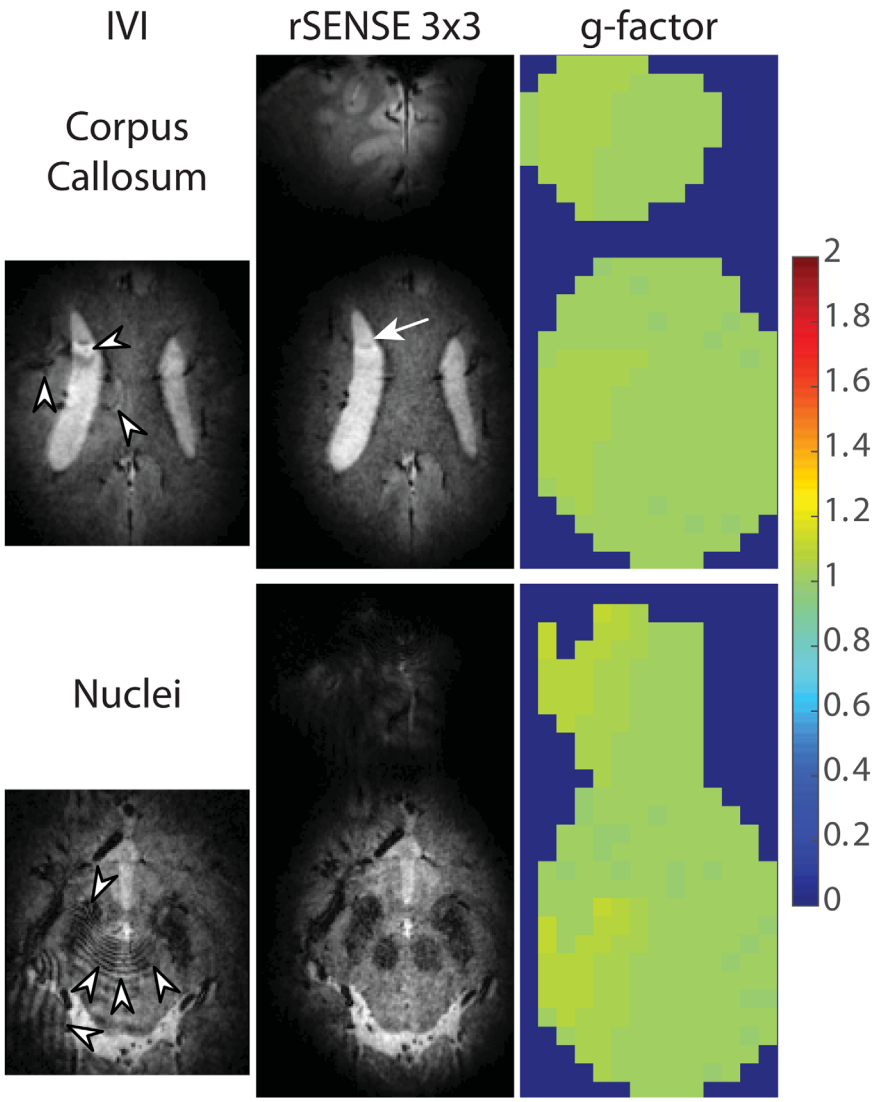

FIG. 8. Images of rFOX shape 2 acquired using IVI and equivalent rSENSE acceleration factor. Transverse reconstructed slices showing the corpus callosum and red nuclei are shown, as well as g-factor maps for both locations. The rSENSE images and g-factor maps are cropped around the signal generating areas. Arrow and arrow heads point to aliasing artifacts.

Testing the Robustness and Flexibility of rSENSE

To demonstrate the robustness of rSENSE toward an imperfect rFOX, we designed rFOX shape 2 to have a separate excitation hotspot in addition to the first rFOX shape. In Figure 8, we see that the purposely introduced signal hotspot leads to several artifacts due to signal folding in the IVI images. When rSENSE is used, the location of the hotspot is revealed, and most of the aliasing artifacts are avoided. One artifact is greatly reduced in visibility, but is still present in the rSENSE image (white arrow). The g-factor remains close to 1, indicating little to no SNR loss with respect to an rSENSE acquisition of rFOX shape 1.

An excitation pattern following the outer cortex (rFOX shape 3) is absolutely incompatible with IVI. Figure 9 shows that rFOX can still be used to speed up the acquisition of this rFOX shape, whereas simply unfolding this scan using the default full FOX coil sensitivity map leads to obvious artifacts. In this situation, the number of signal contributing voxels was halved with respect to the full FOX, but an rSENSE acceleration factor of $3 \times 3 = 9$ could be used.

DISCUSSION

This work proposed to combine rFOX with SENSE into rSENSE. By using rFOX in the coil sensitivity mapping procedure, information on the actual aliasing voxels can be provided to the unfolding algorithms, resulting in high quality images at ultrahigh acceleration factors.

The receive coil sensitivity scans combined well with the 2D spatially selective RF pulses that were used to create the rFOX. Voxels that were not excited were excluded from SENSE unfolding and the remaining voxels were successfully reconstructed. The extended TR in the sensitivity mapping scans lead to an increase in scan time of these scans, from 66 s in the regular 1D-selective scan to 148 s for rFOX shapes 1 and 2 and 324 s for rFOX shape 3. On one hand, one could argue that an

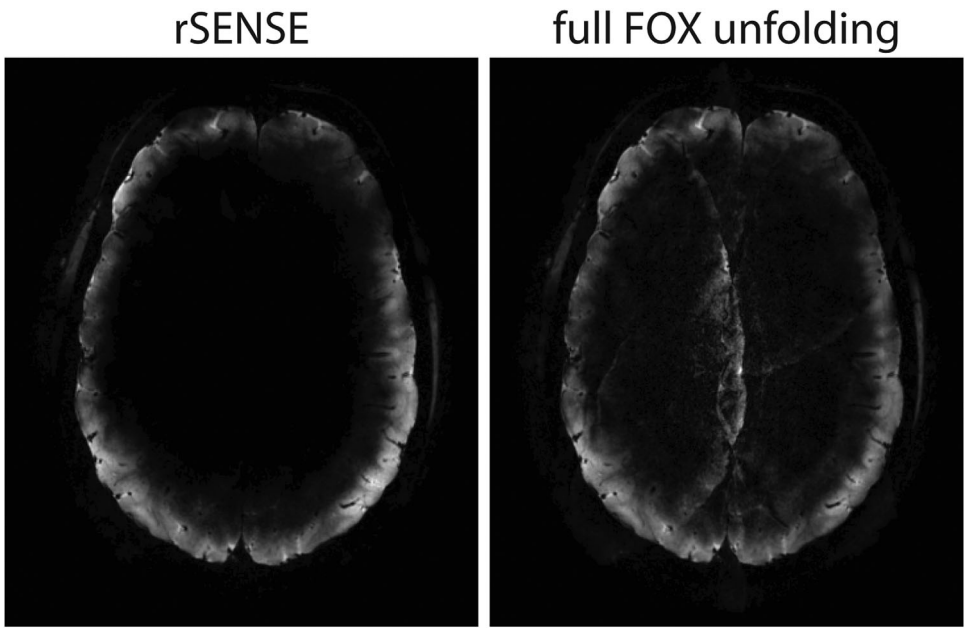

FIG. 9. PI accelerated (AF = 3 × 3), T_2^* weighted, transverse reconstructed images of rFOX shape 3, exciting the outer cortex. The images were reconstructed using rSENSE (left) and using the coil sensitivities of the full FOX (right).

increased calibration scan time is permitted if the actual (functional) scan can be performed faster, or using shorter echo times. On the other hand, other strategies for providing information of the rFOX could be envisaged that would require less scan time in the calibration phase of the scan protocol. For example, the targeted or simulated excitation pattern might be used as a mask on the regular full FOX coil sensitivity map.

The newly proposed rSENSE method clearly performed better than regular SENSE when imaging a limited region of interest, as was predicted by a drastically reduced g-factor. At acceleration factors above the rFOV limit, regular SENSE creates unusable images while rSENSE results in excellent images in the corpus callosum and usable images in the red nuclei.

When rFOX is combined with SENSE acceleration and a full FOX coil sensitivity scan, image quality is also improved significantly with respect to regular SENSE, but is not as good as rSENSE. This reduction in image quality is likely due to the incorrect unfolding of signal to voxels that did not contribute any to the aliased image.

When an imperfect rFOX was simulated, we saw that rSENSE was capable of unfolding most of the extra signal to its origin, where in IVI this lead to aliasing. This exemplifies the robustness of rSENSE compared with IVI, and is, therefore, the preferred method. A prerequisite for this to work is that the location of the imperfection is known in the unfolding process. It can be measured during the coil sensitivity mapping, or the simulated excitation pattern might be used as a mask on the regular full FOX coil sensitivity map. However, it remains to be determined to what extent a discrepancy between the simulated rFOX and the actual one could result in large reconstruction errors. In our example, one aliasing artifact was not completely removed. The spatial location of this signal was probably masked out in the reconstruction due to partial volume effects at the edge of the rFOX.

Several other methods of achieving a reduced field of excitation are available, such as refocusing slices orthogonal to excitation (2), outer volume suppression with spatial saturation (25), and signal localization by means of violation of the CPMG conditions (26). The rSENSE method should work with either of these rFOX generating methods, but providing the voxels exclusion information may not be as straightforward as with 2D RF pulses. In these cases, a regular 1D selective coil sensitivity map might be used that is masked by the targeted or simulated rFOX.

GRAPPA uses autocalibration of the coil sensitivity during each sequence, possibly simplifying the process of performing rFOX-matched reconstructions. However, because GRAPPA operates in the k-space domain, an exact exclusion of silent voxels is not possible and the benefits of having fewer contributing voxels are not immediately clear. Still, certain benefits have been shown empirically (11–13).

A previously explored strategy of using SENSE acceleration after applying IVI (27) should be identical to rSENSE when the rFOX perfectly matches the rFOV. In this approach, there is no need to provide additional rFOX knowledge to the SENSE reconstruction, because this is implicitly supplied by defining the rFOV. However, one can no longer benefit from the robustness towards excitation errors offered by rSENSE and one is limited to rFOX shapes that perfectly match the (usually square shaped) rFOV.

When rSENSE is considered to be used for accelerating an existing scan protocol, a short optimization of this protocol should be performed by determining the excitation target area, obtaining coil sensitivity maps and calculating g-factors for different acceleration factors. This is an additional effort to be performed before starting a new study that focusses on a particular region of interest, but results in a more effective scan protocol of which the cumulative benefits will be paramount when applied to a large number of examinations.

In practice, voxel exclusion in SENSE unfolding is achieved through regularization instead of masking, as is clearly explained by Omer and Dickinson (28). There are no obvious reasons why this would not be compatible with rFOX inclusion in the coil sensitivity maps. In fact, the performance of rSENSE might benefit from this method because it lacks a sharp transition between excluded and included voxels, as is the case with masking.

CONCLUSIONS

We have shown how an rFOX is imaged most effectively: by combining rFOX and SENSE into rSENSE. Compared with SENSE of the full FOX, higher acceleration factors can be obtained. Compared with IVI, the rSENSE method offers greater geometrical flexibility and additional scan acceleration facilitated by PI.

REFERENCES

1. Mooiweer R, Sbrizzi A, Raaijmakers A, van den Berg CAT, Luijten PR, Hoogduin H. Squashing the g-factor: ultra high scan acceleration factors in reduced field of excitation imaging. In Proceedings of the 23rd Annual Meeting of ISMRM, Toronto, Canada, 2015. Abstract 3620.
2. Feinberg D, Hoenninger JC, Crooks L, Kaufman L, Watts J, Arakawa M. Inner volume MR imaging: technical concepts and their application. Radiology 1985;156:743–747.
3. Sodickson DK, Manning WJ. Simultaneous acquisition of spatial harmonics (SMASH): Fast imaging with radiofrequency coil arrays. Magn Reson Med 1997;38:591–603.
4. Pruessmann KP, Weiger M, Scheidegger MB, Boesiger P. SENSE: sensitivity encoding for fast MRI. Magn Reson Med 1999;42:952–962.
5. Pfeuffer J, Van De Moortele P-F, Yacoub E, Shmuel A, Adriany G, Andersen P, Merkle H, Garwood M, Ugurbil K, Hu X. Zoomed functional imaging in the human brain at 7 Tesla with simultaneous high spatial and high temporal resolution. Neuroimage 2002;17:272–286.
6. Griswold MA, Jakob PM, Chen Q, Goldfarb JW, Manning WJ, Edelman RR, Sodickson DK. Resolution enhancement in single-shot imaging using simultaneous acquisition of spatial harmonics (SMASH). Magn Reson Med 1999;41:1236–1245.
7. Rieseberg S, Frahm J, Finsterbusch J. Two-dimensional spatially-selective RF excitation pulses in echo-planar imaging. Magn Reson Med 2002;47:1186–1193.
8. Schneider R, Haueisen J, Pfeuffer J. Shaped saturation with inherent radiofrequency-power-efficient trajectory design in parallel transmission. Magn Reson Med 2014;72:1015–1027.
9. Mooiweer R, Sbrizzi A, El Aidi H, Eikendal ALM, Raaijmakers A, Visser F, van den Berg CAT, Leiner T, Luijten PR, Hoogduin H. Fast 3D isotropic imaging of the aortic vessel wall by application of 2D spatially selective excitation and a new way of inversion recovery for black blood imaging. Magn Reson Med 2016;75:547–555.
10. Heidemann R, Fasano F, Vogler M, Leuze C, Pfeuffer J, Turner R. Improving image quality by combining outer volume supression and parallel imaging: zoomed EPI with GRAPPA at 7T. In Proceedings of the 16th Annual Meeting of ISMRM, Toronto, Canada, 2008. Abstract 1284.
11. Heidemann RM, Anwander A, Feiweier T, Knösche TR, Turner R. k-space and q-space: combining ultra-high spatial and angular resolution in diffusion imaging using ZOOPPA at 7 T. Neuroimage 2012;60:967–978.
12. Heidemann RM, Ivanov D, Trampel R, Fasano F, Meyer H, Pfeuffer J, Turner R. Isotropic submillimeter fMRI in the human brain at 7 T: Combining reduced field-of-view imaging and partially parallel acquisitions. Magn Reson Med 2012;68:1506–1516.
13. Coristine AJ, van Heeswijk RB, Stuber M. Combined T 2 -preparation and two-dimensional pencil-beam inner volume selection. Magn Reson Med 2015;74:529–536.
14. Gallichan D, Marques JP, Gruetter R. Retrospective correction of involuntary microscopic head movement using highly accelerated fat image navigators (3D FatNavs) at 7T. Magn Reson Med 2016;75:1030–1039.
15. Taviani V, Alley MT, Banerjee S, Nishimura DG, Daniel BL, Vasanawala SS, Hargreaves BA. High-resolution diffusion-weighted imaging of the breast with multiband 2D radiofrequency pulses and a generalized parallel imaging reconstruction. Magn Reson Med 2017;77:209–220.
16. van den Brink JS, Watanabe Y, Kuhl CK, et al. Implications of SENSE MR in routine clinical practice. Eur J Radiol 2003;46:3–27.
17. Weiger M, Pruessmann KP, Boesiger P. 2D SENSE for faster 3D MRI. MAGMA 2002;14:10–19.
18. Griswold MA, Jakob PM, Heidemann RM, Nittka M, Jellus V, Wang J, Kiefer B, Haase A. Generalized autocalibrating partially parallel acquisitions (GRAPPA). Magn Reson Med 2002;47:1202–1210.
19. Pauly J, Nishimura D, Macovski A. A k-space analysis of small-tip-angle excitation. J Magn Reson 1989;81:43–56.
20. Grissom W, Yip C, Zhang Z, Stenger VA, Fessler JA, Noll DC. Spatial domain method for the design of RF pulses in multicoil parallel excitation. Magn Reson Med 2006;56:620–629.
21. Zwanenburg JJM, Versluis MJ, Luijten PR, Petridou N. Fast high resolution whole brain T2* weighted imaging using echo planar imaging at 7T. Neuroimage 2011;56:1902–1907.
22. Sbrizzi A, Hoogduin H, Lagendijk JJ, Luijten P, Sleijpen GLG, van den Berg CAT. Time efficient design of multi dimensional RF pulses: application of a multi shift CGLS algorithm. Magn Reson Med 2011;66:879–885.
23. Nehrke K, Versluis MJ, Webb A, Börnert P. Volumetric B_1^+ mapping of the brain at 7T using DREAM. Magn Reson Med 2014;71:246–256.
24. Lin F-H, Kwong KK, Belliveau JW, Wald LL. Parallel imaging reconstruction using automatic regularization. Magn Reson Med 2004;51:559–567.
25. Le Roux P, Gilles RJ, McKinnon GC, Carlier PG. Optimized outer volume suppression for single-shot fast spin-echo cardiac imaging. J Magn Reson Imaging 1998;8:1022–1032.
26. Malik SJ, Hajnal JV. Phase relaxed localized excitation pulses for inner volume fast spin echo imaging. Magn Reson Med 2016;76:848–861.
27. Wargo CJ, Gore JC. Rapid acquisition of targeted high resolution human brain images using a combined SENSE, inner volume imaging, and multishot EPI spin echo sequence at 7T. In Proceedings of the 19th Annual Meeting of ISMRM, Montreal, Canada, 2011. Abstract 2358.
28. Omer H, Dickinson R. Regularization in parallel MR image reconstruction. Concepts Magn Reson Part A 2011;38A:52–60.